On the influence of liquid/vapor phase change onto the Nusselt number of a laminar superheated or subcooled vapor flow

Elena Roxana Popescu, Sébastien Tanguy, Catherine Colin

On the influence of liquid/vapor phase change onto the Nusselt number of a laminar superheated or subcooled vapor flow

Elena-Roxana Popescu*, Sébastien Tanguy**, Catherine Colin

Institut de Mécanique des Fluides de Toulouse (IMFT), Université de Toulouse, CNRS, Toulouse, France

Keywords:
Film vaporization/condensation
Heat transfer
Boundary layer flow
Nusselt number
Friction coefficient

A B S T R A C T

Based on a numerical approach, we propose in this study to characterize the interaction between a laminar boundary layer of a superheated or subcooled vapor flow and a static liquid pool at saturation temperature. For the purpose of this study, we define a canonical configuration that will help to improve our physical understanding of the interaction between a laminar flow and vaporization or condensation. By performing a full set of simulations sweeping the parameters space, correlations are proposed for the first time on the Nusselt number depending on the dimensionless numbers (the Reynolds number, the Prandtl number, the Jakob number and the density ratio) that characterize both vaporization and condensation. As attended, the Nusselt number decreases or increases in the configurations involving vaporization or condensation respectively. For high Jakob number, opposite trends are observed depending whether if vaporization or condensation is considered. Indeed a saturation of the heat flux happens in the first case, whereas a self-amplification of the heat flux occurs in the second one. Since the Nusselt number expressions are known, analytical expressions for the integrated heat flux exchanged at the liquid/vapor interface can be determined. Our study also takes interest to the behaviour of the viscous friction of the vapor flow on the liquid pool, which is weakly affected by the phase change, despite the important variation of the local flow structure due to evaporation or condensation. The physical mechanisms inducing all these phenomena are here discussed and clarified.

1. Introduction

There is currently little information on how an external flow will modify evaporation or condensation of a liquid plane surface in spite of its significant interest in various fields, such as processes in thermal engineering, in combustion applications, weather forecasting or climate modeling. Most applications cited above involve turbulent flows and gas mixture. Nevertheless, the simpler configuration where a laminar superheated or subcooled vapor flow is shearing a saturated liquid interface has still never been solved whether theoretical, numerical or experimental approaches are considered. This would be a significant step forward before considering more complex configurations. The theory of an expanding laminar boundary layer of a fluid above a solid plate, known as the Blasius theory [1], has been generalized to account for heat transfer between the fluid and an isothermal plate by Pohlhausen in Ref. [21]. Both theories are based on a boundary layer hypothesis assuming that the velocity component in the streamwise direction is much higher than the one in the normal direction to the plate. However, when one considers an expanding boundary layer of a superheated or subcooled vapor flow over a saturated liquid, the latter assumption is no longer valid due to the phase change vapor flow that will respectively blow or aspirate the boundary layer, depending on whether vaporization or condensation occurs. The mathematical complexity of this problem being strongly increased, the resulting flow will exhibit a fully two-dimensional rotational structure for which a classical theoretical analysis can hardly be practiced. Consequently, using fully resolved numerical simulation is a promising alternative for tackling such a problem in order to improve our knowledge in the field of heat transfer in liquid-vapor flow with phase change. Phase change heat transfer, treated using the so-called conception of the two-phase boundary layer, has been a subject of study in several papers. For example, Koh et al. made an analysis of a saturated vapor in a forced-convection flow over a flat plate in Ref. [12] and a vertical plate in Ref. [13]. The configuration with film boiling was studied for a forced-convection flow by Cess and Sparrow in Ref. [4] and for a free-convection flow by Kaneyasu and Takehiro in Ref. [11]. Turkyilmazoglu in Ref. [32] studies the traditional Stefan problems concerning solidification or liquidisation phenomena of a phase changing bar. Regarding

* Corresponding author.
** Corresponding author.
E-mail addresses: epopescu@imft.fr (E.-R. Popescu), tanguy@imft.fr (S. Tanguy).

https://doi.org/10.1016/j.ijthermalsci.2019.02.046

the interaction between liquid-vapor phase change and two-phase flows, s ince t he s eminal w orks o f R enksizbulut a nd Y uen [23,24], where correlations on Nusselt number and drag coefficient of evaporating droplets have been designed, a few studies have been dedicated to fully characterize other configurations.

Scriven [27] has proposed 1D theory of bubble growth involving an induced phase change flow motion (radial and irrotational flow). In the context of bubble growth, Ruckenstein and Davis [25] have developed a theoretical study where the external flow is approximated by a potential flow. Nevertheless, rotational effects can have influence both on the viscous friction and the heat flux as it is the case in the present study.

In this paper, we present a numerical study to characterize the interaction between a superheated or subcooled external laminar vapor flow shearing a static and plane liquid pool at saturation temperature. The Blasius-Pohlhausen theory of an expanding laminar boundary layer over an isothermal plate can be considered as a reference solution. Our purpose was to find, for this configuration, a correlation on the Nusselt number accounting for the modification of the local thermal gradient on the interface due to the vaporization or condensation induced flow. As the local structure of the flow is also modified in the vicinity of the liquid-vapor interface, our study includes an analysis on the interfacial viscous friction when phase change occurs.

To the best of our knowledge, the study on the interaction between an external vapor flow and the liquid/vapor phase change of a liquid pool has never been conducted before in the proposed configuration. In addition to its academic interest, this study could also be relevant in more industrial configurations, as for example in space applications. In launchers fuel tanks, the pressure regularization is done by injecting vapor jets above a liquid plane. It is of utmost importance to predict the vaporization or condensation mass flow rate in such a configuration. A solution is to solve the flow only on a small region close to the liquid/vapor interface and obtain local laws on the heat flux that could be used as a closure model in larger scale approaches.

2. Numerical methods for the direct numerical simulation

2.1. Mathematical formulation

The model used to compute the process of heat transfer with phase change is identical to one described in Refs. [10,31], where the liquid and the vapor phases are supposed incompressible and monocomponent. It is assumed that the fluid d ensities a nd t he thermophysical properties in each phase are spatially uniform. Therefore, the mathematical formulation of the two-phase incompressible flow is:

$$\nabla\cdot\mathbf{V} = 0, \tag{1}$$

$$\rho\frac{D\mathbf{V}}{Dt} = -\nabla p + \nabla\cdot(2\mu\mathbf{D}) + \rho\mathbf{g}. \tag{2}$$

where V is the velocity field, p is the pression field, ρ is the density, μ is the dynamic viscosity, D is the deformation tensor and g is the gravity acceleration.

The thermal field is computed by solving a simplified conservation energy equation, formulated using the enthalpy primitive variable:

$$\rho C_p\left(\frac{DT}{Dt}\right) = \nabla\cdot(k\nabla T), \tag{3}$$

where T is the thermal field, C_p is the specific heat at constant pressure and k is the thermal conductivity.

The governing equations are formulated in a "Jump Condition Form", meaning that the field equations are written in each phase separately and additional jump conditions have to be imposed at the interface to maintain the conservation of mass (Eq. (4)), momentum (Eq. (5)) and energy (Eq. (6)). The movement of expansion or suction in the vapor, depending on whether vaporization or condensation occurs, is directly related to the phase change mass flow rate,

$$[\mathbf{V}]_\Gamma = \dot{m}\left[\frac{1}{\rho}\right]_\Gamma \mathbf{n}. \tag{4}$$

Because of the interface motion, momentum in the direction of the unit normal vector **n** is convected at the relative velocity of the fluid with respect to the interface. Including the effects of the pressure and surface tension forces, the momentum balance normal to the interface writes

$$[p]_\Gamma = \sigma\kappa + 2\left[\mu\frac{\partial V_n}{\partial n}\right]_\Gamma - \dot{m}^2\left[\frac{1}{\rho}\right]_\Gamma. \tag{5}$$

Finally, the balance of energy at the interface translates that the thermal flux exchanged at the interface depends on the energy released or absorbed in the process of phase change,

$$[-k\nabla T\cdot\mathbf{n}]_\Gamma = \dot{m}L, \tag{6}$$

with σ the surface tension, κ the local interface curvature, **n** the normal vector at the interface pointing towards the liquid phase, L the latent heat of vaporization, $\dot{m}$ the phase change rate and $\frac{\partial V_n}{\partial n}$ the normal derivative of the normal velocity component. The operator $[\cdot]_\Gamma$ accounts for the jump across the interface Γ and it is defined by: $[f]_\Gamma = f_{vap} - f_{liq}$.

The formalism to deduce the jump equations (4)–(6) is described in Appendix A (see Refs. [7,8,19]).

As in this paper we consider a plane interface, simulations results do not depend on surface tension due to zero interface curvature. Moreover, according to the second law of thermodynamics and assuming that the local equilibrium hypothesis is still valid, the interface temperature is imposed at the saturation temperature. This assumption is thermodynamically consistent with a pure liquid/vapor system, see for instance the following reference [3].

2.2. Numerical methods

In this section, the methods used in our numerical study are presented. The dimensional Navier Stokes equations (1)–(6) are solved for a steady incompressible two-phase flow in a two-dimensional domain.

Thermal field is computed by solving the simplified conservation energy Eq. (3). As the liquid-gas interface is not boundary fitted with computational grid, the suitable jump conditions can be imposed across the interface following the general guidelines of the Ghost Fluid Method [6] to maintain the conservation of mass [19,30] and energy [7,8,31]. That is made possible by using the subgrid location of the interface with a static Level Set function whose zero level curve represents the interface [20]. Spatial derivatives are computed with fifth order WENO-Z schemes [2]. A Black-Box MultiGrid solver [5] is used to solve the pressure Poisson equation and we perform an implicit temporal discretization of the viscous terms as presented in Refs. [15,16]. The system of unsteady equations is solved until reaching a steady state by using a second order TVD Runge-Kutta scheme for the temporal integration.

As the interface temperature is constant and continuous across the interface, the following algorithm, named GFTSB (Ghost Fluid Thermal Solver for Boiling) in Refs. [31,34], has been designed in Ref. [7] to solve the heat transfer around the interface when phase change occurs. The scheme used for solving the energy equation is given by

$$\frac{T^{n+1} - T^n}{\Delta t} + \mathbf{u}^n\cdot\nabla T^n = \nabla\cdot(k\nabla T^{n+1}) \tag{7}$$

First, solve the temperature field in the liquid domain with a prescribed Dirichlet boundary condition at the interface

$$\begin{aligned}&\rho_l C_{p_l} T_l^{n+1} - \Delta t\nabla\cdot(k_l\nabla T_l^{n+1}) = \rho_l C_{p_l}(T_l^n - \Delta t\mathbf{u}_l^n\cdot\nabla T_l^n), \text{ if } \phi > 0\\ &T|_\Gamma = T_{sat}\end{aligned} \tag{8}$$

with ϕ the Level Set function. Next, solve the temperature field in the vapor domain with the same prescribed Dirichlet boundary condition at

the interface

$$\rho_v C_{p_v} T_v^{n+1} - \Delta t \nabla \cdot (k_v \nabla T_v^{n+1}) = \rho_v C_{p_v} (T_v^n - \Delta t \mathbf{u}_v^n \cdot \nabla T_v^n), \quad \text{if } \phi < 0$$
$$T|_\Gamma = T_{sat} \tag{9}$$

Once the temperature field has been computed, the local mass flow rate can be easily deduced from

$$\dot{m} = \frac{[-k \nabla T \cdot \mathbf{n}]_\Gamma}{L_{vap}} \tag{10}$$

Given that the temperature field in the liquid is uniform and equal to the saturation temperature, the thermal flux in the liquid phase is zero. The local mass flow rate depends therefore only on the thermal flux in the vapor phase. This formalism allows switching naturally from vaporization to condensation depending only on the sign of the thermal gradient. Indeed, if the vapor is superheated $\dot{m}$ is positive and this leads to a blowing effect in the vapor phase. On the other hand, if the vapor is subcooled, $\dot{m}$ becomes negative which generates an aspirating flow towards the interface.

Our in house code, *DIVA*, has been extensively validated with theoretical solutions [9,31,34] and with experimental data whether Nucleate Boiling [10,33] or Leidenfrost Droplet [26] is considered. Successful comparisons between numerical simulations and experimental data in Ref. [29] for droplets collisions or in Ref. [14] for oscillations of rising bubbles or droplets have also been reported.

3. Computational configuration of numerical simulations

3.1. Initialization and boundary conditions

We consider here the canonical configuration of an expanding Blasius-Pohlhausen boundary layer interacting with a saturated and static liquid pool. Our aim is to investigate the influence of the external flow on the local heat flux, for an improved knowledge on the interaction between liquid/vapor phase change and fluid mechanics. Even though each different industrial system would require a specific quantitative study, there is a strong interest in understanding local mechanisms in academic configurations. A possible experimental set-up representative of our computations is illustrated in Fig. 1.

The actual computational domain implemented in our simulations is the liquid/vapor domain (for $x \geq x_L$). The interface has a plane shape, which corresponds to the asymptotic case of a high Weber number (high surface tension value). The vapor stream is flowing in the upper part of the domain over a static saturated liquid pool located in the lower part of the computational domain. An inflow boundary condition is used on the left of the domain for the injection of the superheated or subcooled vapor flow. Given that the purpose of this work is to study the influence of the liquid/vapor phase change on an expanding Blasius-Pohlhausen boundary layer, a boundary layer thickness δ_{x_L} has to be imposed at the inlet of the domain. This boundary layer thickness depends on the length of the solid plate, defined as x_L on the schematics in Fig. 1. It should be emphasized that the results of the present study will directly depend on the inlet boundary layer thickness δ_{x_L}. Such a dependence on the boundary layer thickness is classical in Fluid Mechanics and has been observed for various type of flows as reported in Refs. [17,18] in the framework of primary atomization, for instance.

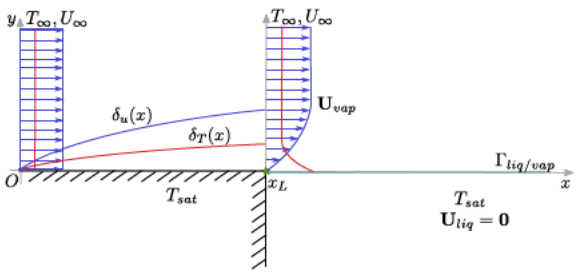

Fig. 1. Schematics of the expanding Blasius-Pohlhausen boundary layer interacting with a saturated and static liquid pool.

Velocity and temperature inflow profiles are computed by solving respectively the Prandtl [22] and the Pohlhausen [21] boundary layer equations:

$$f'''(\eta) + \frac{1}{2} f(\eta) f'(\eta) = 0, \tag{11}$$

and

$$\theta''(\eta) + \frac{Pr}{2} f(\eta) \theta'(\eta) = 0 \tag{12}$$

where $f = \frac{u}{U_\infty}$ and $\theta = \frac{T - T_{sat}}{\Delta T}$ are the normalized stream function and the non-dimensional temperature, respectively; ΔT is the thermal gradient. The boundary conditions are: $\eta = 0$: $f = 0, f' = 0$; $\eta \to \infty$: $f' = 1$ for Eq. (11) and $\eta = 0$: $\theta = 0$; $\eta \to \infty$: $\theta = 1$ for Eq. (12). We recall that $\eta \sim \frac{y}{\delta}$ is the dimensionless variable, $\delta \sim \sqrt{\frac{\nu x}{U_\infty}}$ is the boundary layer thickness, $Pr = \frac{\mu C_p}{k}$ is the Prandtl number.

Free-boundary condition is used on top and on the right of the computational domain, in order to avoid containment effects and to maintain isobaric conditions.

As the aim of this work is to characterize a steady solution of the interaction between an external flow and a static liquid pool, it is considered that the interface position is fixed in time in order to maintain a constant liquid height in the computational domain. This assumption is fitting with the schematics of a possible experimental set-up proposed in Fig. 1, if one considers an additional device that allows maintaining a constant liquid level in the liquid pool. Unlike boiling, stationary hypothesis is a classical approximation [28] when considering the evaporation of a liquid (as droplet evaporation for instance) interacting with a superheated vapor since the velocity of the vapor flow is much higher than the interface speed regression.

Moreover, it has been verified that for viscosity ratios $\frac{\mu_{liq}}{\mu_{vap}} \in [2,56]$ the liquid motion due to the shear stress of the vapor flow on the interface can be neglected in our configurations. Consequently, only the velocity jump condition due to phase change will interact with the external flow. However, such a configuration is consistent with the static liquid hypothesis only if one assumes a sufficiently high density ratio, since the ratio between the interface velocity and the vapor velocity on the interface is close to the density ratio.

The velocity and thermal field are initialized, in the whole domain, with the Blasius-Pohlhausen dynamic and thermal boundary layer profiles, respectively.

3.2. Computational domain and mesh grid

To avoid the thermal singularity on the phase change mass flow rate at the inlet plane, we assume that the vapor flow has traveled a distance x_L over an isothermal solid plate before contacting the liquid pool (Fig. 2 and Fig. 3). Consequently, the boundary layer thickness of the vapor inlet flow depends on this distance x_L that can be accounted for in our dimensionless analysis by defining an inlet Reynolds number Re_{x_L}, such as $Re_{x_L} = \frac{\rho_v U_\infty x_L}{\mu_v}$. The dimensions of the computational domain are (l_x, l_y) with $l_x = 6.7\delta_{x_L}$, $\delta_{x_L} = min(\delta_u, \delta_T)$ where $\delta_u = 4.92\frac{x_L}{\sqrt{Re_{x_L}}}$ and $\delta_T = \delta_u Pr^{-\frac{1}{3}}$ are the dynamic and the thermal boundary layers, respectively. Our interest is to compute the spatial development of the thermal and dynamical boundary layers over the saturated liquid pool. A study on containment effects allowed showing that, for the vaporization configuration, the dimension in the normal direction has to be $l_y = 2l_x$, while, in the condensation configuration, $l_y = l_x$ is sufficient to ensure that the numerical solutions do not depend on the computational domain size. That can be explained considering that the vaporization has a "blowing" effect on the boundary layer and so a larger

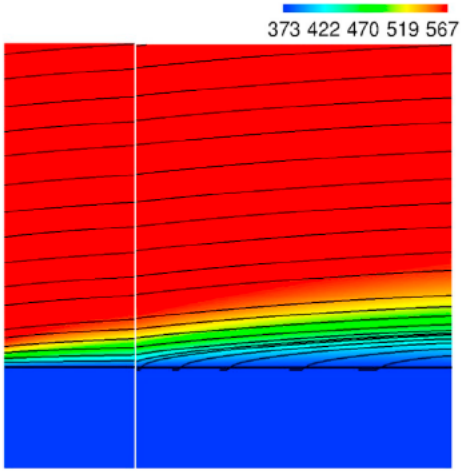

Fig. 2. Streamlines and temperature profile [K] of a liquid pool evaporating in an superheated gas flow for $Pr = 0.98$, $Re_{x_L} = 211$, $\frac{\rho_l}{\rho_v} = 1623$, $Ja_{vap} = 7.38$; left - classic Blasius boundary layer, right - the boundary layer blown by the vaporization.

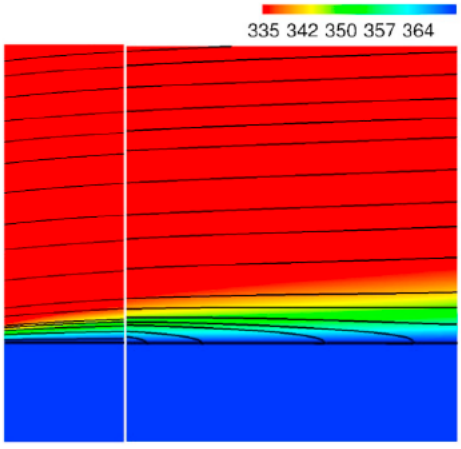

Fig. 3. Streamlines and temperature profile [K] of a subcooled gas flow condensating in the liquid pool. for $Pr = 0.98$, $Re_{x_L} = 211$, $\frac{\rho_l}{\rho_v} = 1623$, $Ja_{cond} = 0.74$; left - classic Blasius boundary layer, right - the boundary layer "aspirated" by the condensation.

domain in the y-direction is needed to assure that the development of the boundary layer is not affected by the upper boundary condition. Unlike vaporization, condensation aspirates the boundary layer, so containement effects have smaller influence on its spatial development.

Even though the present parametric study has been conducted using the computation configuration presented in Section 3.1., some additional verifications have been done to ensure that the upstream containment effects do not have a significant influence on the Nusselt number evolution (Fig. B.16 in B).

A convergence study with different mesh grids has been carried out for both configurations, for a couple of liquid/vapor defined by the following dimensionless numbers: $Pr = 1.022$, $Re_{x_L} = 85.726$, $\frac{\rho_l}{\rho_v} = 17.746$, and two different values for the Jakob number: $Ja_{vap} = 3.69$ and $Ja_{vap} = 8.87$ for the vaporization and $Ja_{cond} = 0.37$ and $Ja_{cond} = 1.15$ for the condensation. The dimensionless numbers are defined as it follows: $Re_x = \frac{\rho_v U_\infty x}{\mu_v}$, , $Ja_{vap} = \frac{C_{p_v}(T_\infty - T_{sat})}{L}$ and $Ja_{cond} = \frac{C_{p_v}(T_{sat} - T_\infty)}{L}$. The subscript '$v$' is for vapor and '$l$' is for liquid, μ is the viscosity, C_{p_v} is the specific heat, k is the thermal conductivity, $T_v - T_{sat}$ is the thermal gradient and U_∞ is the velocity in the uniform zone outside the boundary layer.

The local dimensionless coefficient of heat transfer, known also as the local Nusselt number, is defined as

$$Nu_x = \frac{hx}{k} = \frac{\phi_l x}{k(T_l - T_\infty)}, \tag{13}$$

where h is the convective heat transfer coefficient, ϕ_l is the local heat flux at the liquid/vapor interface and T_l is the liquid/vapor interface temperature, equal to the saturation temperature T_{sat}.

At first glance, the evolution of the Nusselt number seems to be converged with the grid 256×256, for the vaporization (Fig. 4) and with the grid 128×128 for the condensation configuration (Fig. 5). Nevertheless, the velocity jump at $x = x_L$ from a single-phase boundary layer flow to a phase change boundary layer flow has to be captured and well resolved. As one of the objectives of this numerical study is to define correlations on the Nusselt number, high accuracy is required. Consequently, the mesh grid 2048×1024 - for the vaporization, and 1024×1024 - for the condensation have been chosen to run the present numerical study. At the inlet, this mesh grid allows to have ~ 150 points in the boundary layer.

Since all the simulations are 2D and reach a steady state, the overall computational cost of one simulation remains moderate even if a very refined grid is considered. This has permitted to perform a full parametric study by varying the four dimensionless numbers characterizing

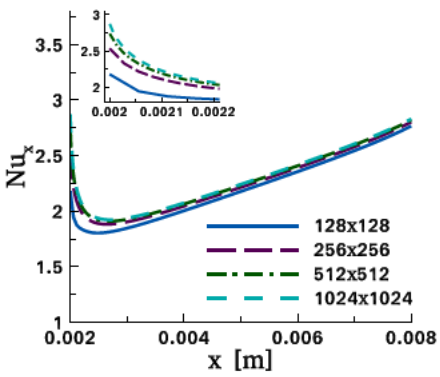

(a) $Ja = 3.69$

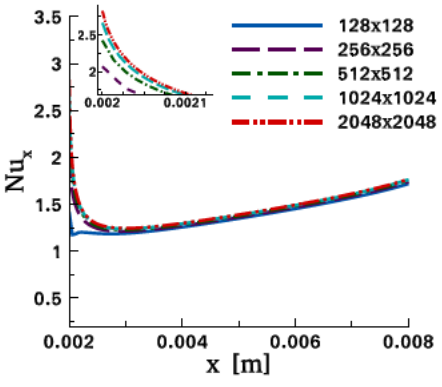

(b) $Ja = 8.87$

Fig. 4. Convergence study for the evolution of the Nusselt number for the vaporization configuration, for the dimensionless numbers: $Re_{x_L} = 85.726$, $Pr = 1.022$, $\frac{\rho_l}{\rho_v} = 17.746$.

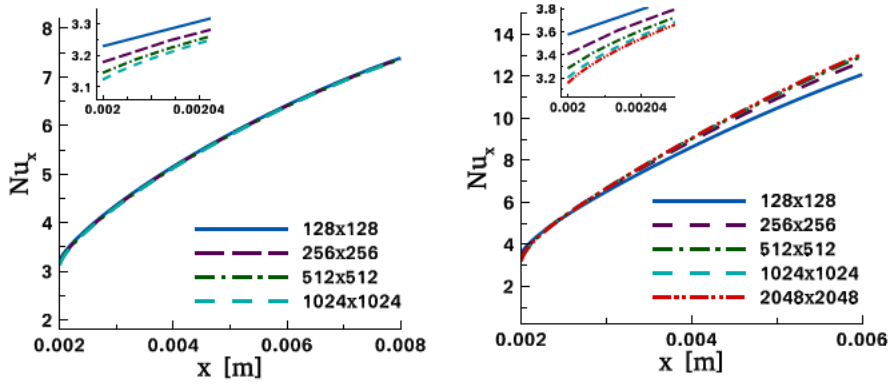

(a) $Ja = 0.37$ (b) $Ja = 1.15$

Fig. 5. Convergence study for the evolution of the Nusselt number for the condensation configuration, for the dimensionless numbers: $Re_{x_L} = 85.726$, $Pr = 1.022$, $\frac{\rho_l}{\rho_v} = 17.746$.

our configuration in a wide range of values. Moreover, solving mass and momentum conservation equations in the liquid field enabled us to assess that neglecting the liquid motion was a correct assumption, for high viscosity ratio.

4. Results and discussion

4.1. Parametric study

A parametric study has been conducted to determine how the Nusselt number is varying with the dimensionless numbers characterizing our configuration. These dimensionless numbers can be extracted from the physical model as: the Reynolds number Re_x from the momentum balance Eq. (2), the Prandtl number Pr from the energy conservation equation Eq. (3), the Jakob number Ja from the balance of energy at the interface Eq. (6) and the density ratio $\frac{\rho_l}{\rho_v}$ from the jump condition on the mass conservation Eq. (4).

The physical variables varied in this parametric study are the velocity U_∞ for the Reynolds number, the thermal conductivity of the vapor k for the Prandtl number, the latent heat L for the Jakob number and the liquid density ρ_l for the density ratio.

The range of values for our parametric study was: $Re_{x_L} = (15; 1250)$, $Pr = (0.6; 8)$, $Ja = (0.00037; 8.87)$ and $\frac{\rho_l}{\rho_v} = (10; 5000)$, with approximately fifty simulations in both configurations.

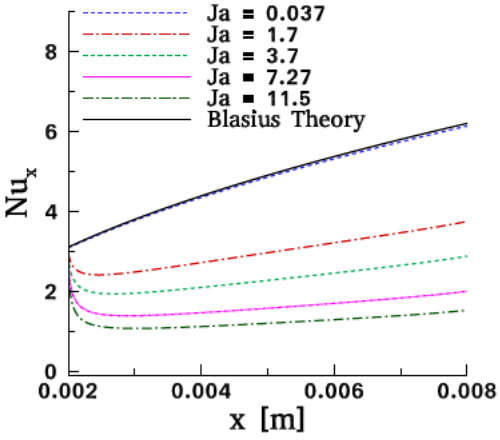

Fig. 6. Spatial evolution of the Nusselt number for different Jakob number for the vaporization configuration; $Pr = 1.022$, $Re_{x_L} = 85.726$, $\frac{\rho_l}{\rho_v} = 17.746$.

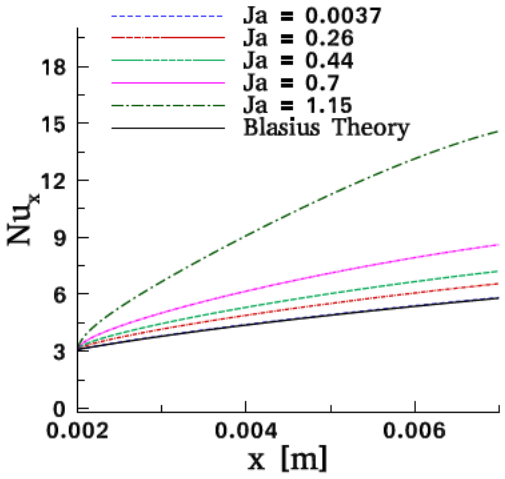

Fig. 7. Spatial evolution of the Nusselt number for different Jakob number for the condensation configuration; $Pr = 1.022$, $Re_{x_L} = 85.726$, $\frac{\rho_l}{\rho_v} = 17.746$.

4.2. The spatial evolution of the Nusselt number

The spatial evolution of the Nusselt number along the longitudinal coordinate x is showed in Fig. 6 for vaporization, and in Fig. 7 for condensation, with a couple of liquid/vapor defined by the following dimensionless numbers: $Pr = 1.022$, $Re_{x_L} = 85.726$, $\frac{\rho_l}{\rho_v} = 17.746$, and different values of Jakob number. One can see that the Nusselt number is lower for vaporization and higher for condensation than the Nusselt number obtained from the Blasius theory. Indeed, as observed in Fig. 2, when vaporization occurs, the thermal boundary layer being thickened due to the expansion flow of vapor, the heat transfer coefficient decreases. The same trend has been observed by Yan and Soong in Ref. [35], where the convective heat and mass transfer along an inclined heated plate with film evaporation have been studied. On the other hand, the condensation involves an aspirating flow towards the liquid/vapor interface, as it can be visualized in Fig. 3. As this flow decreases the thermal boundary layer thickness, the heat transfer coefficient is increased.

For the vaporization, the minimum value observed on the Nusselt number can be related to the rapid decrease of the heat flux in the vicinity of the inlet flow (see Fig. 8). This can be explained by the connecting zone between the Blasius-Pohlhausen expanding boundary layer (for $x < x_L$) and the established flow in interaction with the phase change (for $x >> x_L$).

The influence of the Jakob number on the spatial evolution of the Nusselt number can also be visualized in Figs. 6 and 7. The increase of

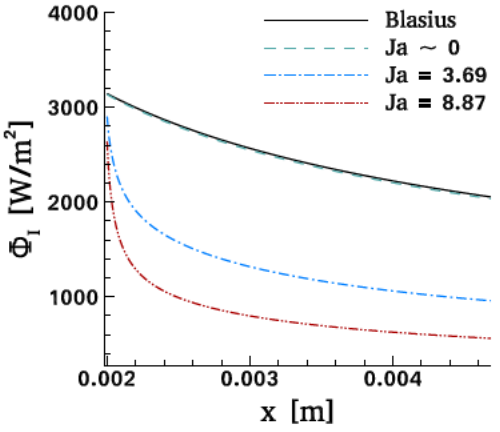

Fig. 8. Vaporization Configuration - Evolution of the local heat flux ϕ_I with the x-axis for the dimensionless numbers: $Pr = 1.022$, $Re_{x_L} = 85.726$, $\frac{\rho_l}{\rho_v} = 17.746$ and different values of Jakob number.

the Jakob number implies an increase of the vapor/liquid phase change and therefore the Nusselt number decreases or increases if vaporization or condensation is respectively concerned, as expected. Figs. 6 and 7 are now compared in regard to the influence of the Jakob number on the Nusselt number evolution. If the Jakob number is doubled and then tripled, in the case of the boundary layer "blown" by the liquid pool vaporization, a decrease of the intervals between the succesives curves is observed, while if the boundary layer is "aspirated" by the condensation, the intervals between the succesives curves increase. These unanticipated results will be further explained, but first, the correlations on the Nusselt number will be presented.

4.3. Correlations on the Nusselt number

By fitting the numerical Nusselt number evolution obtained in all of our simulations, we have found, general correlations that depend on the dimensionless numbers characterizing this configuration. In what follows, the resulting correlations are presented separately for the vaporization and for the condensation. For the sake of simplicity, the approach to find these correlations is described in the Appendix C. Both correlations have been designed by adding correction terms to the Nusselt number from the Blasius theory which is defined as $Nu_x^{Bl} = 0.332 Pr^{0.333} Re_x^{0.5}$.

4.3.1. Vaporization

The correlation for the Nusselt number with vaporization has the following expression

$$Nu_x^{vap} = Nu_x^{Bl} - \left(\alpha\left(\frac{x}{x_L} - 1\right)^n + \beta\right) H(x - x_L), \tag{14}$$

where $H(x - x_L)$ is the Heaviside function who has a non-zero value only for $x > x_L$, α, β and n have the following expressions

$$\alpha = 0.294 Re_{x_L}^{0.495} Pr^{0.333} \left(1 - e^{-0.0248\left(Ja\left(\frac{\rho_l}{\rho_v} - 1\right)\right)}\right),$$

$$n = 0.935 Re_{x_L}^{-0.11} Pr^{-0.07} Ja^{-0.1} \frac{\rho_l}{\rho_v}^{-0.12},$$

$$\beta = 0.119 Re_{x_L}^{0.477} Pr^{0.237} \left(1 - e^{-0.0043 Ja\left(\frac{\rho_l}{\rho_v} - 1\right)}\right),$$

4.3.2. Condensation

In the configuration involving condensation, the correlation on the Nusselt number writes as

Table 1
The average relative error and the maximum relative error for the Nusselt number for different couples of dimensionless numbers.

	Condensation	$\bar{\epsilon}$[%]	ϵ_{max}[%]
C.1	$Pr = 8$, $Re_{x_L} = 85.726$, $Ja = 0.37$, $\frac{\rho_l}{\rho_v} = 17.6$	1.028	1.171
C.2	$Pr = 0.98$, $Re_{x_L} = 1250$, $Ja = 0.179$, $\frac{\rho_l}{\rho_v} = 1623$	0.58	0.75
C.3	$Pr = 1.022$, $Re_{x_L} = 85.726$, $Ja = 0.7$, $\frac{\rho_l}{\rho_v} = 17.6$	0.65	1.34
C.4	$Pr = 0.98$, $Re_{x_L} = 105.51$, $Ja = 0.179$, $\frac{\rho_l}{\rho_v} = 5000$	0.28	0.32
C.5	$Pr = 0.98$, $Re_{x_L} = 30$, $Ja = 0.179$, $\frac{\rho_l}{\rho_v} = 1623$	1.38	1.6
C.6	$Pr = 6$, $Re_{x_L} = 105.51$, $Ja = 0.179$, $\frac{\rho_l}{\rho_v} = 1623$	1.69	1.8
C.7	$Pr = 0.98$, $Re_{x_L} = 105.51$, $Ja = 0.29$, $\frac{\rho_l}{\rho_v} = 1623$	0.57	0.703
	Vaporization	$\bar{\epsilon}$[%]	ϵ_{max}[%]
V.1	$Pr = 8$, $Re_{x_L} = 85.726$, $Ja = 3.69$, $\frac{\rho_l}{\rho_v} = 17.6$	1.56	7
V.2	$Pr = 0.98$, $Re_{x_L} = 1250$, $Ja = 0.179$, $\frac{\rho_l}{\rho_v} = 1623$	1.09	1.45
V.3	$Pr = 1.022$, $Re_{x_L} = 85.726$, $Ja = 8.87$, $\frac{\rho_l}{\rho_v} = 17.6$	2.13	9.4
V.4	$Pr = 0.98$, $Re_{x_L} = 105.51$, $Ja = 0.179$, $\frac{\rho_l}{\rho_v} = 3500$	2.4	2.8
V.5	$Pr = 1.022$, $Re_{x_L} = 30$, $Ja = 3.69$, $\frac{\rho_l}{\rho_v} = 17.6$	4.8	6
V.6	$Pr = 1.022$, $Re_{x_L} = 85.726$, $Ja = 3.69$, $\frac{\rho_l}{\rho_v} = 5$	1.8	2.69
V.7	$Pr = 0.98$, $Re_{x_L} = 105.51$, $Ja = 0.3598$, $\frac{\rho_l}{\rho_v} = 1623$	2.17	2.64

$$Nu_x^{cond} = Nu_x^{Bl} + \left(\gamma\left(\frac{x}{x_L} - 1\right)^m + \eta\right) H(x - x_L), \tag{15}$$

where γ, η and m have the following expressions

$$\gamma = 0.0854 Re_{x_L}^{0.483} Pr^{0.356} \left(e^{0.1018 Ja\left(\frac{\rho_l}{\rho_v} - 1\right)} - 1\right),$$

$$m = 0.519 Re_{x_L}^{-0.045} Pr^{-0.042} e^{0.02985 Ja \frac{\rho_l}{\rho_v}},$$

$$\eta = 0.00042 Re_{x_L}^{0.426} Pr^{0.55} \left(Ja\left(\frac{\rho_l}{\rho_v} - 1\right)\right)^{1.25}.$$

4.3.3. Validation of the proposed correlations

For the sake of validation of the proposed correlations, we present for various configurations in Table 1, the average relative error ε and the maximum relative error ε_{max}, between the computed Nusselt number and the correlations, with the relative error defined as: $\epsilon = \frac{Nu_x^{correl} - Nu_x^{num}}{Nu_x^{num}} 100\%$. One can see that the average relative error between the Nusselt number from DNS and the correlation is less than 2% for condensation and less than 5% for vaporization. Comparisons between the proposed correlations and numerical results are also plotted in Fig. 9 for the vaporization and in Fig. 10 for the condensation for different configurations from Table 1.

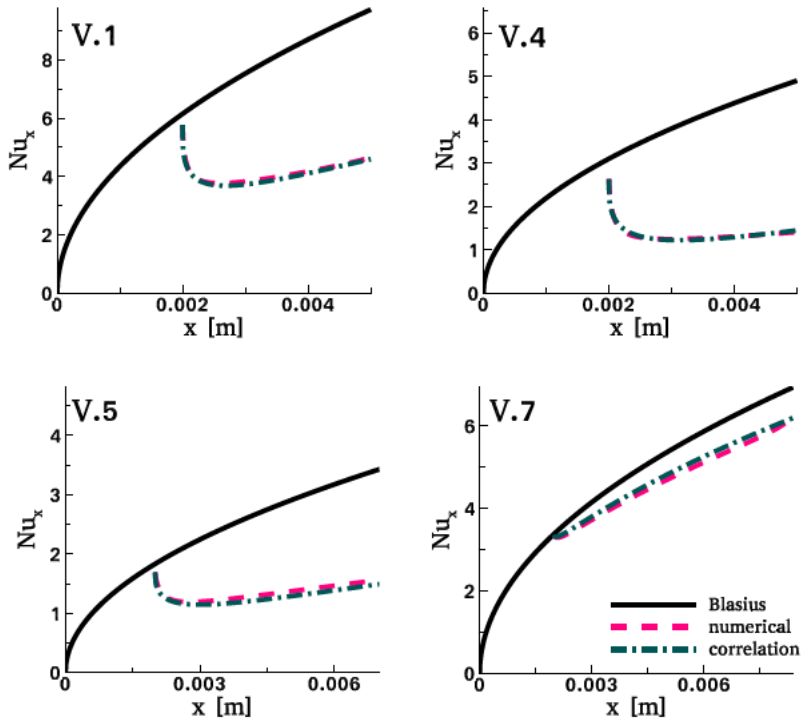

Fig. 9. Spatial evolution of the Nusselt number for different configurations extracted from Table 1 for the case involving vaporization.

4.4. Asymptotic cases

The correlations on the Nusselt number can be simplified when considering asymptotic cases, as it will be shown in the following paragraphs.

4.4.1. Asymptotic cases for the vaporization Nusselt number correlation

If $Ja \rightarrow 0$, the approximation of the terms depending on the Jakob number yields simpler expressions for the parameters α and β from Eq. (14):

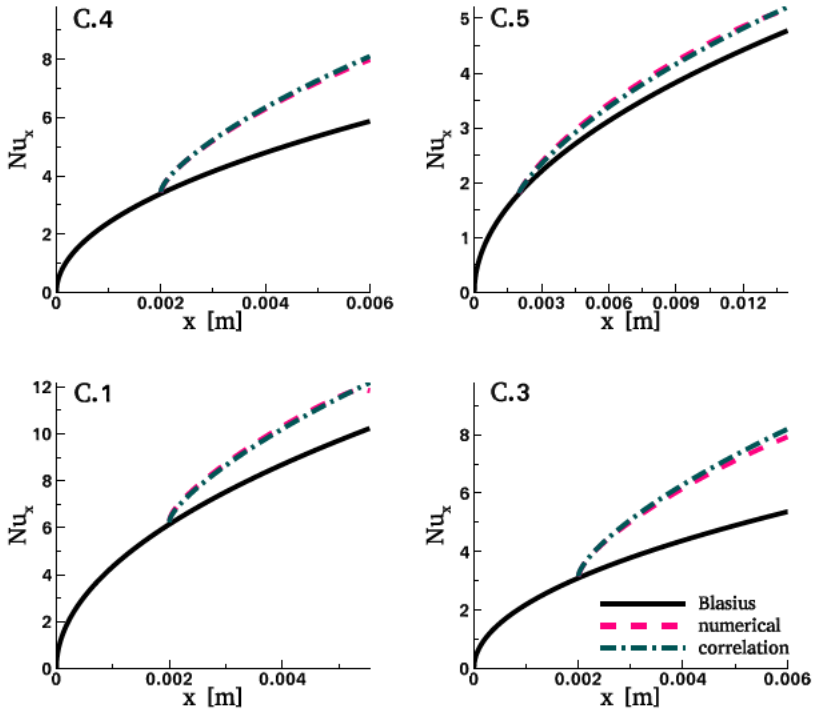

Fig. 10. Spatial evolution of the Nusselt number for different configurations extracted from Table 1 for the case involving condensation.

$$\alpha(Ja \to 0) = 0.0073Ja\left(\frac{\rho_l}{\rho_v} - 1\right)Re_{x_L}^{0.495}Pr^{0.333}$$

and

$$\beta(Ja \to 0) = 0.0005Ja\left(\frac{\rho_l}{\rho_v} - 1\right)Re_{x_L}^{0.477}Pr^{0.237}.$$

This asymptotic case brings out a linear evolution of the Nusselt number, both with the Jakob number and the density ratio, for low vaporization rate.

When $Ja = 0$, the correction terms equal to 0 as the jump condition on the velocity field is zero. Hence, the boundary layers are not modified and the expression of the Nusselt number fits simply with the one obtained with the Blasius theory.

Considering the asymptotic cases $Ja \to \infty$ or $\frac{\rho_l}{\rho_v} \to \infty$, it can be shown that in the vaporization case, the expression of the Nusselt number tends towards a saturation value:

$$Nu_x^{vap}(Ja \to \infty) \to Nu_x^{Bl} - \left(0.294Re_{x_L}^{0.495}Pr^{0.333} + 0.119Re_{x_L}^{0.4777}Pr^{0.2374}\right).$$

It can be explained by remarking that an increase of the vapor superheat tends to increase the local heat flux on the interface, and thus, the jump on the normal velocity. As this jump condition tends to thicken the thermal boundary layer and thus to decrease the local heat flux, the saturation effect results from an equilibrium state between these two antagonistic effects.

4.4.2. Asymptotic cases for the condensation Nusselt number correlation

The expression of the Nusselt number in the condensation case is now presented for a low Jakob number.

If $Ja \to 0$, Eq. (15) becomes:

$$Nu_x^{cond} \simeq Nu_x^{Bl} + \gamma\left(\frac{x}{x_L} - 1\right)^m H(x - x_L),$$

with

$$\gamma(Ja \to 0) = 0.0087Ja\left(\frac{\rho_l}{\rho_v} - 1\right)Re_{x_L}^{0.483}Pr^{0.356}$$

and

$$m(Ja \to 0) = 0.519Re_{x_L}^{-0.045}Pr^{-0.042},$$

considering

$$\eta(Ja \to 0) = 0.$$

As for the vaporization, when $Ja = 0$, the Nusselt number simply fits with the Blasius theory.

Moreover, if $Ja \to \infty$ or $\frac{\rho_l}{\rho_v} \to \infty$, an opposite trend to the one observed for vaporization is reported. In the case of condensation, the oncoming subcooled flow being aspirated towards the interface, the thickness of the thermal boundary layer is reduced. This leads to an increase of the local heat transfer as it can be visualized in Fig. 7. It is found that in the case of condensation, no saturation effect on the Nusselt number is observed neither in the numerical simulations, nor in the expression of the proposed correlation 15. This can be understood by remarking that, compared to vaporization, in the case of condensation, the jump condition on the normal velocity is of opposite direction, favoring the local heat transfer. These trends have also been observed when Figs. 6 and 7 were compared regarding to the influence of the Jakob number on the evolution of the Nusselt number.

4.5. The integrated heat flux

From the correlations on the Nusselt number one can calculate the expression of the integrated heat flux exchanged at the liquid/vapor interface.

4.5.1. Vaporization

Given the expression (eq. (14)) of the Nusselt number when vaporization happens, the heat flux per unit of width, integrated between x_L and x is defined as

$$\Phi^{vap}(x, x_L) = \int_{x_L}^{x} \phi^{vap}(x)dx = k(T_\infty - T_{sat})\int_{x_L}^{x} \frac{Nu^{vap}(x)}{x}dx$$
$$= k(T_\infty - T_{sat})\left(\int_{x_L}^{x} \frac{Nu^{Bl}(x)}{x}dx - \alpha\int_{x_L}^{x} \frac{\left(\frac{x}{x_L} - 1\right)^n}{x}dx - \beta\int_{x_L}^{x} \frac{1}{x}dx\right) \tag{16}$$

The different components of eq. (16) are calculated as it follows

$$\int_{x_L}^{x} \frac{Nu^{Bl}(x)}{x}dx = 2(Nu^{Bl}(x) - Nu^{Bl}(x_L)), \tag{17}$$

$$\int_{x_L}^{x} \frac{\left(\frac{x}{x_L} - 1\right)^n}{x}dx = \frac{\left(\frac{x}{x_L}\right)^n {}_2F_1\left(-n, -n; 1 - n, \frac{x_L}{x}\right)}{n} - \pi\csc(\pi n), \tag{18}$$

where $\csc(\pi n) = \frac{1}{\sin(\pi n)}$ is the cosecant function and ${}_2F_1\left(-n, -n; 1 - n; \frac{x_L}{x}\right)$ is the Gauss hypergeometric function, defined as

$${}_2F_1(a, b; c; z) = \frac{\Gamma(c)}{\Gamma(a)\Gamma(b)}\sum_{k=0}^{\infty}\left(\frac{\Gamma(a + k)\Gamma(b + k)}{\Gamma(c + k)}\frac{z^k}{k!}\right)$$

with $\Gamma(a) = (a - 1)!$ the gamma function.

If one considers also the region $x \in (0, x_L)$ where the boundary layer is evolving without interacting with the vaporization, one will find the following expression for the heat flux per unit of width

$$\Phi(x, x_L) = \int_0^{x_L} \phi^{Bl}(x)dx + \int_{x_L}^{x} \phi^{vap}(x)dx = k(T_\infty - T_{sat})\Bigg\{2Nu^{Bl}(x) -$$
$$- \left[\alpha\left(\frac{\left(\frac{x}{x_L}\right)^n {}_2F_1\left(-n, -n; 1 - n, \frac{x_L}{x}\right)}{n} - \pi\csc(\pi n)\right) + \beta\ln\left(\frac{x}{x_L}\right)\right]H(x - x_L)\Bigg\} \tag{19}$$

The expression (eq. (19)) of the integrated heat flux is plotted in Fig. 11. The black curve represents the integrated flux exchanged if the boundary layer evolved without interacting with the liquid vaporization. The dotted lines depict the x-evolution of the thermal flux exchanged at the liquid/vapor interface from x_L to L_x for different values of the Jakob number. As expected, the vaporization reduces the exchanged heat flux.

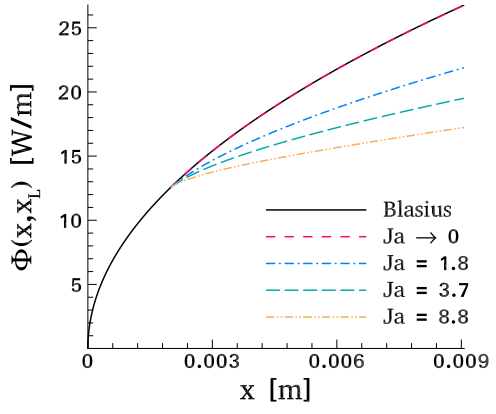

Fig. 11. The x-evolution of the integrated exchanged thermal flux at the interface for $Pr = 1.022$, $Re_{x_L} = 85.726$, $\frac{\rho_l}{\rho_v} = 17.746$ and different values of the Jakob number - vaporization configuration.

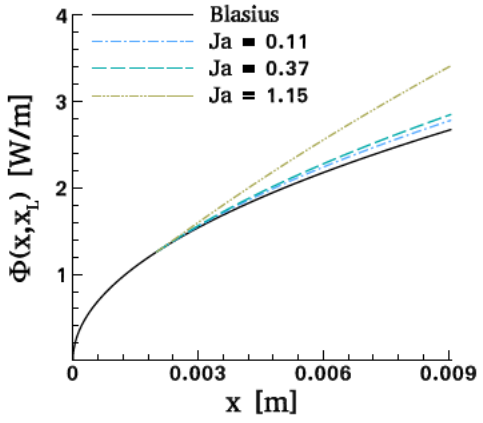

Fig. 12. The x-evolution of the integrated exchanged thermal flux at the interface for $Pr = 1.022$, $Re_{x_L} = 85.726$, $\frac{\rho_l}{\rho_v} = 17.746$ and different values of the Jakob number - condensation configuration.

4.5.2. Condensation

For the configuration with condensation, the approach to calculate the exchanged heat flux is the same as for the vaporization. Considering the expression (eq. (15)) of the Nusslet number, the exchanged heat flux per unit of width is expressed as

$$\Phi(x, x_L) = \int_0^{x_L} \phi^{Bl}(x)dx + \int_{x_L}^{x} \phi^{cond}(x)dx = k(T_\infty - T_{sat})\Bigg\{2Nu^{Bl}(x)+ \\ + \left[\gamma\left(\frac{\left(\frac{x}{x_L}\right)^m {}_2F_1\left(-m,-m;1-m,\frac{x_L}{x}\right)}{m} - \pi\csc(\pi m)\right) + \eta\ln\left(\frac{x}{x_L}\right)\right]H(x - x_L)\Bigg\} \tag{20}$$

The evolution of the integrated heat flux is plotted in Fig. 12. The black curve represents the integrated flux exchanged if the boundary layer evolved without interacting with the condensation. The dotted lines depict the x-evolution of the exchanged heat flux at the liquid/vapor interface from x_L to L_x for different values of the Jakob number. The exchanged heat flux is increased by the condensation.

4.6. The influence of the phase change on the viscous friction

We now examine the influence of the liquid/vapor phase change on the viscous friction. Given the expression of the viscous tensor:

$$\bar{\bar{\tau}} = \begin{pmatrix} 2\mu\frac{\partial u}{\partial x} & \mu\left(\frac{\partial u}{\partial y} + \frac{\partial v}{\partial x}\right) \\ \mu\left(\frac{\partial u}{\partial y} + \frac{\partial v}{\partial x}\right) & 2\mu\frac{\partial v}{\partial y} \end{pmatrix}$$

we know that at the interface of normal vector $\mathbf{e}_y$, the stress vector $\mathbf{T} = \bar{\bar{\tau}}\cdot\mathbf{e}_y$ has the following normal and shear components: $\mathbf{T}\cdot\mathbf{e}_y = \mu\frac{\partial v}{\partial y}$ and $\mathbf{T}\cdot\mathbf{e}_x = \mu\left(\frac{\partial u}{\partial y} + \frac{\partial v}{\partial x}\right)$.

The friction coefficient can be determined by: $\frac{C_f}{2} = \frac{\tau_I}{\rho U_\infty^2}$ with the expression of the interfacial friction: $\tau_I = \mathbf{T}\cdot\mathbf{e}_x|_{y_I}$. We recall that for the Blasius theory the friction coefficient is $\frac{C_f^{Bl}}{2} = \frac{0.332}{\sqrt{Re_x}}$. Plotted in Fig. 13 is the evolution of the friction coefficient for the three configurations, i.e. Blasius theory, vaporization and condensation. One can see that, surprisingly, the phase change does not influence the viscous friction at the liquid/vapor interface, despite the modification of the velocity field in the vicinity of the interface.

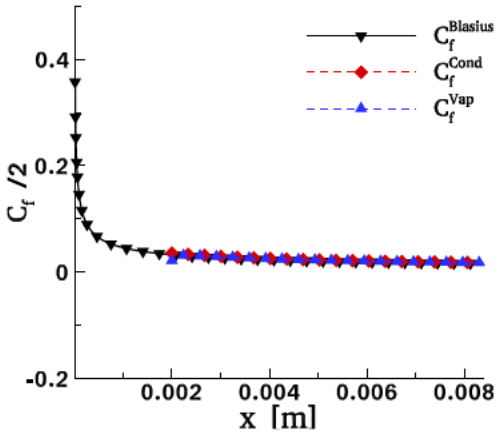

Fig. 13. Evolution of the friction coefficient for: $Pr = 1.022$, $Re_{x_L} = 85.726$, $\frac{\rho_l}{\rho_v} = 17.746$, $Ja_{vap} = 3.69$ and $Ja_{cond} = 0.369$.

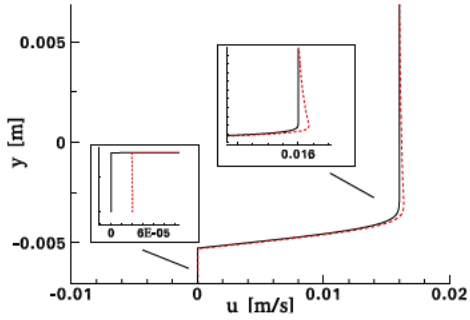

Fig. 14. Evolution of the tangential velocity u for the vaporization study case for $Pr = 1.022$, $Re_{x_L} = 85.726$, $\frac{\rho_l}{\rho_v} = 17.746$, $Ja_{vap} = 3.69$: black line - Blasius theory, red dashed line - vaporization configuration. Zoom on the liquid region (the bottom left) and on the zone close to the interface (middle right).

In order to justify the relevance of this result we will further take a look at the tangential and the normal velocities at the liquid/vapor interface. For the sake of simplicity we will take only the example of the vaporization. In Fig. 14, the evolution of the tangential velocity with the Y-axis is plotted for $x = \frac{l_x}{2}$. It is noteworthy that the evolution of the tangential velocity profile in the vaporization configuration is almost identical to the Blasius boundary layer velocity profile, despite the vapor blowing in the normal direction due to phase change. The liquid motion due to the shear stress of the vapor flow on the interface is negligible (see the zoom at the bottom left of the figure). Moreover, there is little modification of the tangential velocity profile at the liquid/vapor interface (for $y = -0.005$ m) (see the zoom situated in the middle right of the graphics). As simulations showed that we can still make the assuption $\frac{\partial u}{\partial y} \gg \frac{\partial v}{\partial x}$, this explains why only marginal modifications of the interfacial friction coefficient are observed.

Plotted in Fig. 15 is the evolution of the normal velocity v and the thermal flux $\Phi = k_v\frac{\partial T}{\partial y}$ with the Y-axis for a fixed value of x. An important difference can be observed between the normal velocity from the Blasius theory and the normal velocity when the vaporization phenomenon occurs. Unlike the classical Blasius theory, where the thermal flux is induced only by conduction, in the phase change configuration there is a significant influence of the thermal convection in the transverse direction. Thereby, it can be understood that the discontinuity on the Nusselt number is induced by the jump condition on the normal velocity field.

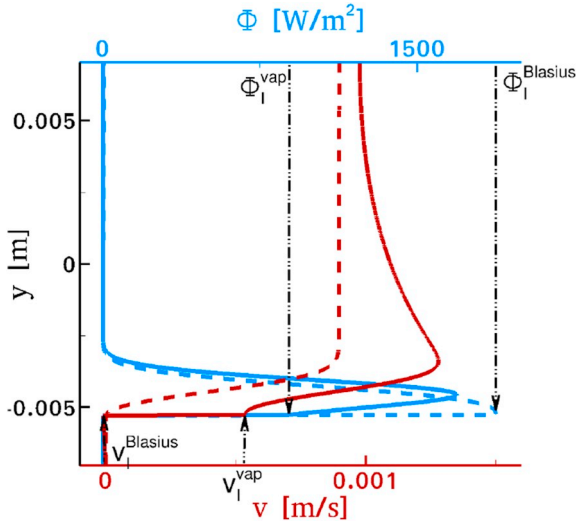

Fig. 15. Evolution of the normal velocity v and the thermal flux Φ for the vaporization study case for $Pr = 1.022$, $Re_{x_L} = 85.726$, $\frac{\rho_l}{\rho_v} = 17.746$, $Ja_{vap} = 3.69$: dashed line - Blasius theory, solid line - vaporization configuration.

5. Conclusions

Based on numerical simulations, in this paper we propose correlations on the influence of an external flow on the vaporization or condensation of a static liquid pool. It is shown that the local flow, induced by the phase change, decreases or increases, respectively, the local heat flux, depending upon vaporization or condensation is considered. For the vaporization configuration it was found that the Nusselt number, and therefore the heat transfer, decreases exponentially with the Jakob number until reaching a saturation value. The opposite trend is observed for the condensation, for which the Nusselt number increases as an exponential function of the Jakob number. Another noteworthy result is about the viscous friction on the interface, or the tangential component of the viscous tensor, which is weakly affected by the phase change in the case of a plane interface. Additionally, given the evolution of the normal velocity v with y, the influence of the phase change on the normal component of the viscous tensor is still very weak in comparison to the tangential one, as it is the case for the classical Blasius boundary layer. Moreover, even if the profiles are not superimposed, it can be qualitatively observed that the derivative $\frac{\partial v}{\partial y}$ is in the same order of magnitude with or without phase change. This is why we can conclude that the liquid vapor phase change has little influence on the components of the viscous stress vector.

Acknowledgements

The authors gratefully acknowledge the CNES and Air Liquid Advanced Technologies for the financial support of the present doctoral study. The authors gratefully acknowledge the French National Research Agency in the frame of the COALA (COndensation And Liquid Atomization) project ANR-15-CE06-0013. The authors gratefully acknowledge the CNRS (Centre National pour la Recherche Scientifique) for funding delegation to Sebastien Tanguy during the year 2017–2018.

Appendix A. Jump conditions

The liquid and the vapor phases are separated by an interface across which the phase change occurs (i.e. the liquid vaporizes into vapor or the vapor condenses into the liquid). The subscripts l and v are used to refer to the liquid and vapor phases, respectively. The interface velocity is denoted by $\mathbf{V}_\Gamma$ and $\mathbf{n}$ is the local unit vector pointing towards the liquid phase. The interface mass flux, $\dot{m}$ is obtained by using the mass conservation across the interface:

$$\dot{m} = \rho_l(\mathbf{V}_l - \mathbf{V}_\Gamma)\cdot\mathbf{n} = \rho_v(\mathbf{V}_v - \mathbf{V}_\Gamma)\cdot\mathbf{n}. \tag{A.1}$$

The jump on the velocity field across the interface can therefore be written as:

$$[\mathbf{V}]_\Gamma = \dot{m}\left[\frac{1}{\rho}\right]_\Gamma \mathbf{n}. \tag{A.2}$$

According to the second law of thermodynamics and assuming that the local equilibrium hypothesis is still valid, the interface temperature is imposed at the saturation temperature: $T_l = T_v = T_{sat}$ at the interface. Integrating Eq. (3) across the interface along with Eq. (A.1) gives the following jump condition for the energy conservation

$$[\rho h(\mathbf{V}_l - \mathbf{V}_\Gamma)\cdot\mathbf{n}]_\Gamma = [-k\nabla T\cdot\mathbf{n}]_\Gamma, \tag{A.3}$$

where the operator $[\cdot]_\Gamma$ accounts for the jump across the interface Γ and it is defined by: $[f]_\Gamma = f_v - f_l$ and h defines the enthalpy. It is assumed that h depends only on the temperature. By using Eq. (A.1), the jump condition for the energy conservation rewrites

$$\dot{m}L = [-k\nabla T\cdot\mathbf{n}]_\Gamma, \tag{A.4}$$

with $L = [h]_\Gamma$ the latent heat of phase change. Finally, integrating Eq. (2) across the interface and including the effects of surface tension leads to:

$$\left[p - \mu\frac{\partial V_n}{\partial n} + \rho(\mathbf{V}\cdot\mathbf{n} - \mathbf{V}_\Gamma\cdot\mathbf{n})^2\right]_\Gamma = \sigma\kappa, \tag{A.5}$$

which, by using Eq. (A.2), is rewritten as

$$[p]_\Gamma = \sigma\kappa + 2\left[\mu\frac{\partial V_n}{\partial n}\right]_\Gamma - \dot{m}^2\left[\frac{1}{\rho}\right]_\Gamma, \tag{A.6}$$

Appendix B. The influence of a conditioning section within the simulation domain

We have included here a graph demonstrating the validity of the inflow boundary condition. A conditioning section has been added, where the

boundary layer is spatially developing from a certain point $x = x_{L_0}$ to $x = x_L$. The phase change is plugged at x_L and we want to investigate the differences between imposing a Blasius profile at the inlet plane and simulating its development upstream. Even if the computation domain starts before the point $x = x_L$, the evolution of the Nusselt number is not affected at all in the far field and only weakly affected in the inlet vicinity, as demonstrated on the figure below.

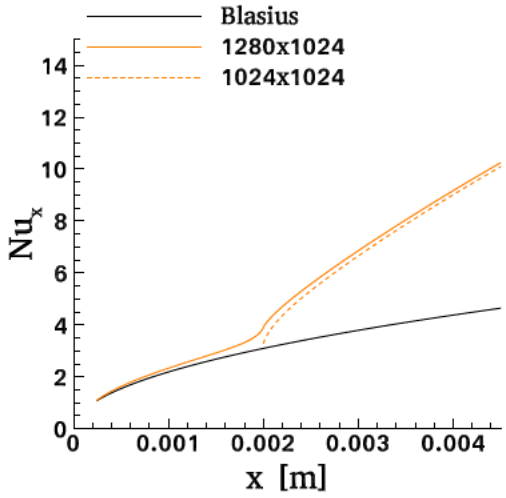

Figure B.16. Spatial evolution of the Nusselt number. Condensation configuration for: $Pr = 1.022$, $Re_{x_L} = 85.726$, $Ja = 1.15$ and $\frac{\rho_l}{\rho_v} = 17.746$.

Appendix C. Parametrical study

The purpose of the present work was to investigate the influence of liquid/vapor phase change on the Blasius theory results, particularly on the Nusselt number evolution. At first, the correction

$$Nu_x^{Bl} - Nu_x^{vap} = F\left(Re_x, Pr, Ja, \frac{\rho_l}{\rho_v}, x_L\right), \tag{C.1}$$

has been plotted.

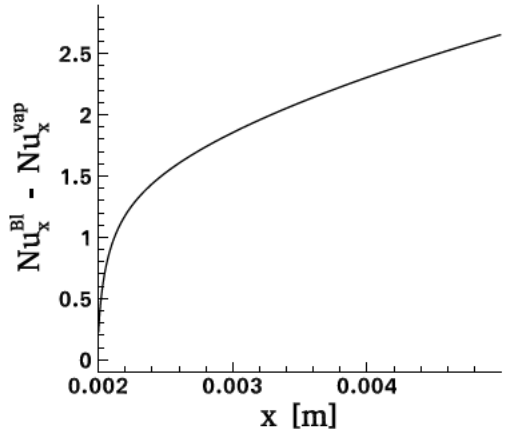

Fig. C.16. The correction on the Nusselt number from the Blasius theory with the x-axis - Vaporization configuration - dimensionless numbers: $Pr = 1.022$, $Re_{x_L} = 85.726$, $Ja = 3.69$ and $\frac{\rho_l}{\rho_v} = 17.746$.

As it can be seen in Fig. C.17, for $x = x_L$, the correction $Nu_x^{Bl} - Nu_x^{vap} \neq 0$ and it increases with x as a power function. Therefore, the Nusselt number with vaporization can be written as

$$Nu_x^{vap} = Nu_x^{Bl} - \left(\alpha\left(\frac{x}{x_L} - 1\right)^n + \beta\right) H(x - x_L), \tag{C.2}$$

where the Heaviside function $H(x - x_L)$ enables locating the phase change only for $x > x_L$.

The next step in our inquiry was to determine the evolution of the parameters α, β and n with the dimensionless numbers characterizing the configuration of interest: Reynolds number Re_{x_L}, Prandtl number Pr, Jakob number Ja and the density ratio $\frac{\rho_l}{\rho_v}$. It is noteworthy that, given the dimensionless form of Eq. (C.2), the choice of an inlet Reynolds number Re_{x_L} instead of a general Reynolds number Re_x is straightforward.

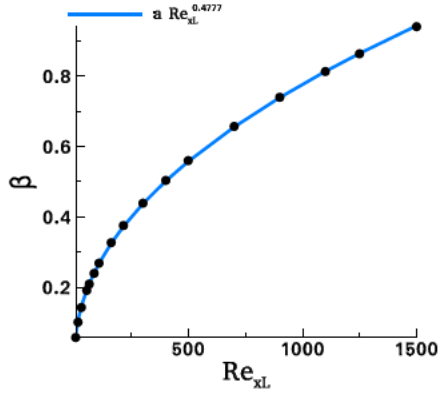

(a) Evolution with the Reynolds number and keeping fixed the dimensionless numbers: $Pr = 1.022$, $Ja = 3.69$ and $\frac{\rho_l}{\rho_v} = 17.746$. // $a(Pr, Ja, \frac{\rho_l}{\rho_v}) = 0.02866$.

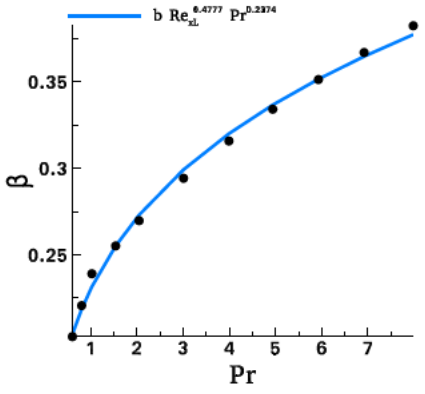

(b) Evolution with the Prandtl number and keeping fixed the dimensionless numbers: $Re_{x_L} = 85.7226$, $Ja = 3.69$ and $\frac{\rho_l}{\rho_v} = 17.746$. // $b(Ja, \frac{\rho_l}{\rho_v}) = 0.0748$.

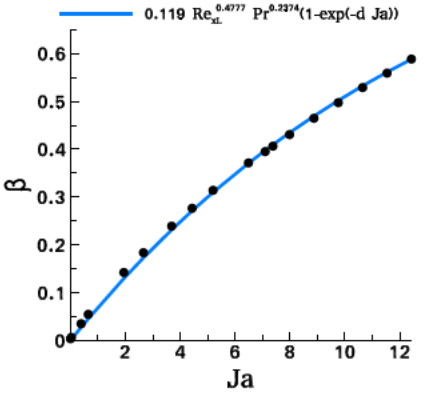

(c) Evolution with the Jakob number and keeping fixed the dimensionless numbers: $Pr = 1.022$, $Re_{x_L} = 85.7226$ and $\frac{\rho_l}{\rho_v} = 17.746$. // $d(\frac{\rho_l}{\rho_v}) = 0.07108$.

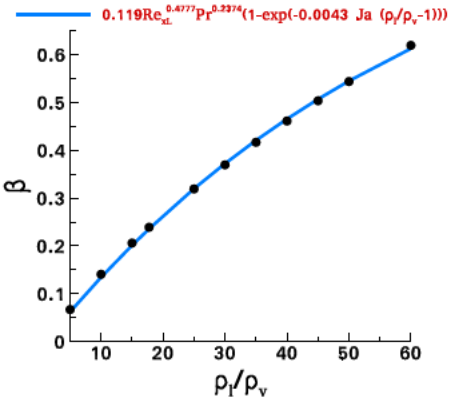

(d) Evolution with the density ratio and keeping fixed the dimensionless numbers: $Pr = 1.022$, $Re_{x_L} = 85.7226$ and $Ja = 3.69$.

Figure C.18. Evolution of the jump $\beta\left(Re_{x_L}, Pr, Ja, \frac{\rho_l}{\rho_v}\right)$ for $x = x_L$ - Vaporization configuration.

The addressed approach to determine the parameters α, β and n is developed as it follows. First, the jump β for $x = x_L$ has been examined. Its evolution with the Reynolds number Re_{x_L} (Fig. C.18a), the Prandtl number (Fig. C.18b), the Jakob number (Fig. C.18c) and finally with the density ratio (Fig. C.18d) have been plotted.

By means of a Matlab library, CFTool, one was able to obtain its evolution with the dimensionless numbers,

$$\beta = 0.119 Re_{x_L}^{0.4777} Pr^{0.2374} \left(1 - exp\left(-0.0043 Ja \left(\frac{\rho_l}{\rho_v} - 1\right)\right)\right).$$

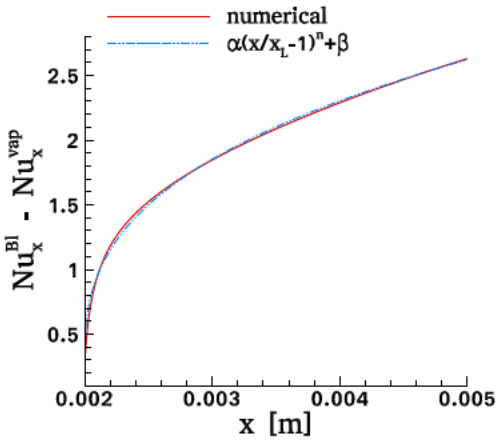

Figure C.19. Spatial evolution of the correction on the Nusselt number from the Blasius theory obtained from the numerical simulation and the function fitting its evolution: $\alpha = 2.062$ and $n = 0.3561$; β known for the corresponding couple of dimensionless numbers.

In the interest of finding the expressions of the parameters α and n from Eq. (C.2), the relation $Nu_x^{Bl} - Nu_x^{vap}$ has been plotted with the x axis for each value of dimensionless number. For example, in Fig. C.19 the evolution of $Nu_x^{Bl} - Nu_x^{vap}$ is plotted for $Re_{x_L} = 85.7226$, $Pr = 1.022$, $Ja = 3.689$, and $\frac{\rho_l}{\rho_v} = 17.746$. Conducting a full set of simulations sweeping a large range of values for the dimensionless numbers enabled us to determine the expressions of parameters α and n,

$$\alpha = 0.294 Re_{x_L}^{0.495} Pr^{0.333} \left(1 - exp\left(-0.0248 Ja \left(\frac{\rho_l}{\rho_v} - 1\right)\right)\right),$$

and

$$n = 0.9351 Re_{x_L}^{-0.11} Pr^{-0.07} Ja^{-0.1} \left(\frac{\rho_l}{\rho_v}\right)^{-0.12}.$$

Their evolution with each dimensionless number is plotted in Fig. C.20 and Fig.C.21.

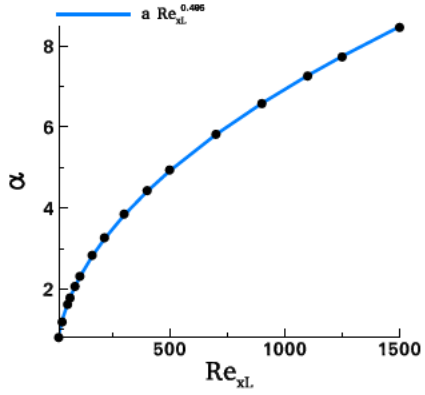

(a) Evolution with the Reynolds number and keeping fixed the dimensionless numbers: $Pr = 1.022$, $Ja = 3.69$ and $\frac{\rho_l}{\rho_v} = 17.746$. // $a(Pr, Ja, \frac{\rho_l}{\rho_v}) = 0.2271$.

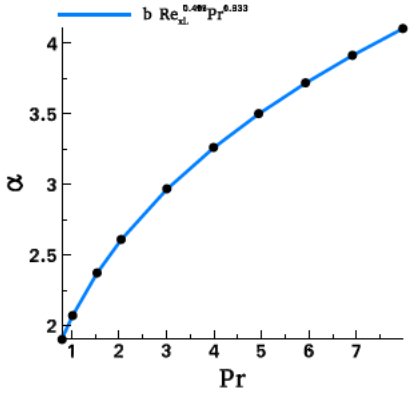

(b) Evolution with the Prandtl number and keeping fixed the dimensionless numbers: $Re_{x_L} = 85.7226$, $Ja = 3.69$ and $\frac{\rho_l}{\rho_v} = 17.746$. // $b(Ja, \frac{\rho_l}{\rho_v}) = 0.227$.

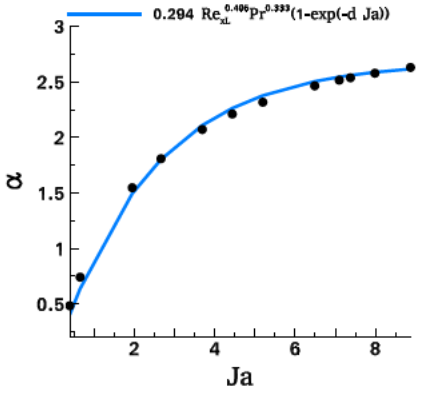

(c) Evolution with the Jakob number and keeping fixed the dimensionless numbers: $Pr = 1.022$, $Re_{x_L} = 85.7226$ and $\frac{\rho_l}{\rho_v} = 17.746$. // $d(\frac{\rho_l}{\rho_v}) = 0.4185$.

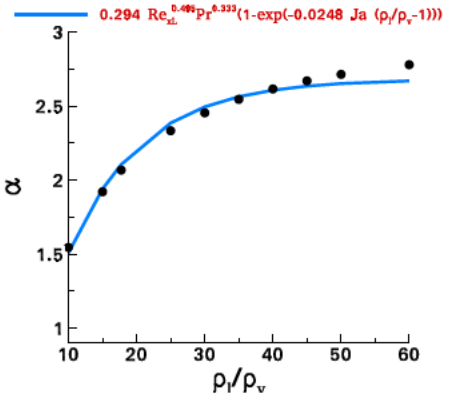

(d) Evolution with the density ratio and keeping fixed the dimensionless numbers: $Pr = 1.022$, $Re_{x_L} = 85.7226$ and $Ja = 3.69$.

Figure C.20. Evolution of the coefficient $\alpha\left(Re_{x_L}, Pr, Ja, \frac{\rho_l}{\rho_v}\right)$ for $x > x_L$ - Vaporization configuration.

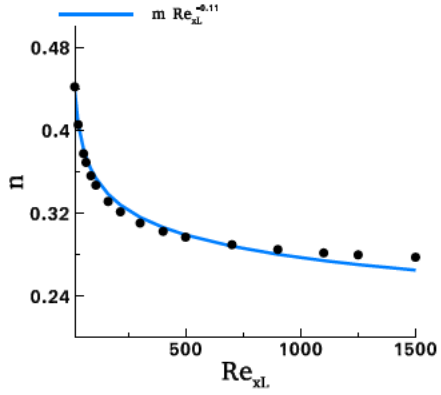

(a) Evolution with the Reynolds number and keeping fixed the dimensionless numbers: $Pr = 1.022$, $Ja = 3.69$ and $\frac{\rho_l}{\rho_v} = 17.746$. // $m(Pr, Ja, \frac{\rho_l}{\rho_v}) = 0.5879$.

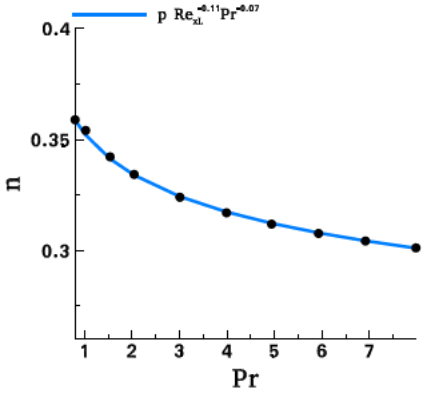

(b) Evolution with the Prandtl number and keeping fixed the dimensionless numbers: $Re_{x_L} = 85.7226$, $Ja = 3.69$ and $\frac{\rho_l}{\rho_v} = 17.746$. // $p(Ja, \frac{\rho_l}{\rho_v}) = 0.5739$.

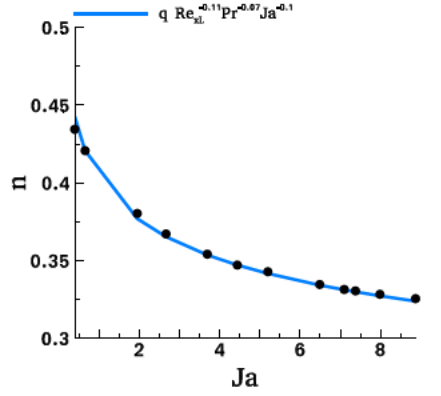

(c) Evolution with the Jakob number and keeping fixed the dimensionless numbers: $Pr = 1.022$, $Re_{x_L} = 85.7226$ and $\frac{\rho_l}{\rho_v} = 17.746$. // $q(\frac{\rho_l}{\rho_v}) = 0.6567$.

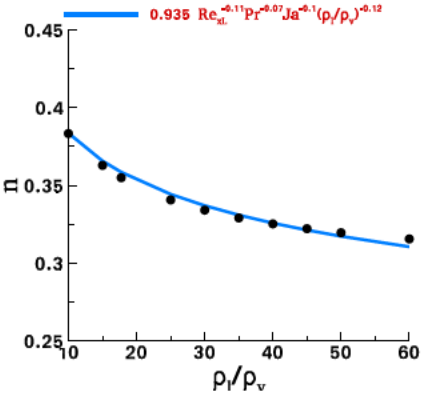

(d) Evolution with the density ratio and keeping fixed the dimensionless numbers: $Pr = 1.022$, $Re_{x_L} = 85.7226$ and $Ja = 3.69$.

Figure C.21. Evolution of the parameter $n\left(Re_{x_L}, Pr, Ja, \frac{\rho_l}{\rho_v}\right)$ for $x > x_L$ - Vaporization configuration.

References

[1] H. Blasius, Grenzschichten in Flüssigkeiten mit kleiner Reibung, Z. Math. u. Phys. 56 (1908) 1–37.

[2] R. Borges, M. Carmona, B. Costa, W. Don, An improved weighted essentially non-oscillatory scheme for hyperbolic conservation laws, J. Comput. Phys. 227 (2008) 3191–3211.

[3] P. Van, Carey. Liquid–Vapor Phase-Change Phenomena, second ed., (2008).

[4] R.D. Cess, E.M. Sparrow, Film boiling in a forced-convection boundary-layer flow, J. Heat Transf. 83 (3) (1961) 370–375.

[5] J.E. Dendy, Black box multigrid, J. Comput. Phys. 48 (1982) 366–386.

[6] R. Fedkiw, T. Aslam, B. Merriman, S. Osher, A non-oscillatory Eulerian approach to interface in multimaterial flows (The Ghost Fluid Method), J. Comput. Phys. 152 (1999) 457–492.

[7] F. Gibou, L. Chen, D. Nguyen, S. Banerjee, A level set based sharp interface method for the multiphase incompressible Navier-Stokes equations with phase change, J. Comput. Phys. 222 (2007) 536–555.

[8] F. Gibou, R. Fedkiw, L.T. Chieng, M. Kang, A second-order-accurate symmetric discretization of the Poisson equation on irregular domains, J. Comput. Phys. 176 (2002) 205–227.

[9] G. Huber, S. Tanguy, J.-C. Bra, B. Gilles, A time splitting projection scheme for compressible two-phase flows. Application to the interaction of bubbles with ultrasound waves, J. Comput. Phys. 302 (2015) 439.

[10] G. Huber, S. Tanguy, M. Sagan, C. Colin, Direct numerical simulation of nucleate pool boiling at large microscopic contact angle and moderate Jakob number, Int. J. Heat Mass Transf. 113 (2017) 662–682.

[11] N. Kaneyasu, I. Takehiro, Two-phase boundary-layer treatment of free-convection film boiling, Int. J. Heat Mass Transf. 9 (1966) 103–115.

[12] J.C.Y. Koh, Film condensation in a forced-convection boundary-layer flow, Int. J. Heat Mass Transf. 5 (1962) 941–954.

[13] J.C.Y. Koh, E.M. Sparrow, J.P. Hartnett, The two phase boundary layer in laminar film condensation, Int. J. Heat Mass Transf. 79 (1961) 69–82.

[14] B. Lalanne, N. Abi Chebel, J. Vejražka, S. Tanguy, O. Masbernat, F. Risso, Non-linear shape oscillations of rising drops and bubbles: experiments and simulations, Phys. Fluids 27 (2015) 123305.

[15] B. Lalanne, L. Rueda Villegas, S. Tanguy, F. Risso, On the computation of viscous terms for incompressible two-phase flows with level Set/Ghost Fluid Method, J. Comput. Phys. 301 (2015) 289–307.

[16] M. Lepilliez, E.-R. Popescu, F. Gibou, S. Tanguy, On two-phase flow solvers in irregular domains with contact line, J. Comput. Phys. 321 (2016) 1217–1251.

[17] P. Marmottant, E. Villermaux, On spray formation, J. Fluid Mech. 498 (2004) 73–111.

[18] J.-P. Matas, A. Delon, A. Cartellier, Shear instability of an axisymmetric air-water coaxial jet, J. Fluid Mech. 843 (2018) 575–600.

[19] D. Nguyen, R. Fedkiw, M. Kang, A boundary condition capturing method for incompressible flame discontinuities, J. Comput. Phys. 172 (2001) 71–98.

[20] S. Osher, J.A. Sethian, Fronts propagating with curvature-dependent speed: algorithms based on Hamilton-Jacobi formulations, J. Comput. Phys. 2 (1988) 12–49.

[21] E. Pohlhausen Der, Wärmeaustausch zwischen festen Körpern und Flüssigkeiten mit kleiner Reibung und kleiner Wärmeleitung, Z. Angew. Math. Mech. 1 (1921) 115–121.

[22] L. Prandtl, über Flüssigkeitsbewegung bei sehr kleiner Reibung, Proc. 3rd Intern. Math. Congr. Heidelberg, 1904, p. 484.

[23] M. Renksizbulut, M.C. Yuen, Experimental study of droplet evaporation in a high temperature stream, J. Heat Transf. 105 (1983) 384–388.

[24] M. Renksizbulut, M.C. Yuen, Numerical study of droplet evaporation in a high temperature stream, J. Heat Transf. 105 (1983) 389–397.

[25] E. Ruckenstein, E.J. Davis, The effects of bubble translation of vapor bubble growth in a superheated liquid, Int. J. Heat Mass Transf. 14 (1971) 939–952.
[26] L. Rueda-Villegas, S. Tanguy, G. Castanet, O. Caballina, F. Lemoine, Direct numerical simulation of the impact of a droplet onto a hot surface above the leidenfrost temperature, Int. J. Heat Mass Transf. 104 (2017) 1090–1109.
[27] L.E. Scriven, On the dynamics of phase growth, Chem. Eng. Sci. 10 (1959) 1–13.
[28] D.B. Spalding, Combustion and Mass Transfer: a Textbook with Multiple-Choice Exercices for Engineering Students, Pergamon Press, Oxford; New York, 1979.
[29] S. Tanguy, A. Berlemont, Application of a level set method for simulation of droplet collisions, Int. J. Multiph. Flow 31 (2005) 1015–1035.
[30] S. Tanguy, T. Menard, A. Berlemont, A level set method for vaporizing two-phase flows, J. Comput. Phys. 221 (2007) 837–853.
[31] S. Tanguy, M. Sagan, B. Lalanne, F. Couderc, C. Colin, Benchmarks and numerical methods for the simulation of boiling flows, J. Comput. Phys. 264 (2014) 1–22.
[32] M. Turkyilmazoglu, Stefan problems for moving phase change materials and multiple solutions, Int. J. Therm. Sci. 126 (2018) 67–73.
[33] A. Urbano, S. Tanguy, G. Huber, C. Colin, Direct numerical simulation of nucleate boiling in micro-layer regime, Int. J. Heat Mass Transf. 123 (2018) 1128–1137.
[34] L. Rueda Villegas, R. Alis, M. Lepilliez, S. Tanguy, A Ghost Fluid/Level Set Method for boiling flows and liquid evaporation: application to the leidenfrost effect, J. Comput. Phys. 316 (2016) 789–813.
[35] W.-M. Yan, C.-Y. Soong, Convective heat and mass transfer along an inclined heated plate with film evaporation, Int. J. Heat Mass Transf. 38 (1995) 1261–1269.